ISSN: 2319-5967
ISO 9001:2008 Certified
International Journal of Engineering Science and Innovative Technology (IJESIT)
Volume 4, Issue 6, November 2015

A Dynamic Simulator Design for Humanoid Robots

Emre Sariyildiz, Hakan Temeltas

Abstract*— This paper proposes a new dynamic simulator for humanoid robots. The exact dynamic model of a humanoid robot is derived by using floating point base dynamics so that the discontinuity problem of the conventional methods is solved. To provide better insight into the dynamic behavior of a humanoid robot, the exact dynamic model is derived by proposing numerical and analytical methods. Although only humanoid robots are considered in this manuscript, the proposal can be similarly applied to different floating point base dynamic systems such as mobile and space robots. A new simulator is designed by using the proposed dynamic model and MATLAB-Simulink. Conventional control engineering schematic diagram is used in the design of the simulator so that users, who have basic control knowledge, can easily adapt it. Not only the controller and trajectory generation but also the model parameters, such as impedance of contact model, can be easily modified by users, i.e., the proposed simulator provides an important design freedom and flexibility to achieve better dynamic model for the actual implementations. Animations of a humanoid robot are obtained by using the Virtual Reality Toolbox (VRT) of MATLAB. Simulation results of the whole body motion control of a humanoid robot are given to show the validity of the proposal.

***Index Terms*— Humanoid Robots, Floating Point Base Dynamics, Locomotion, Simulator Design, Whole Body Motion Control.**

I. INTRODUCTION

Humanoids have several superiorities over other robot systems, e.g., the mechanical structure of a humanoid robot is very useful to perform complicated tasks in humans' daily life environments [1-4]. However, current humanoid robots can perform quite simple tasks, such as walking on an even terrain and are far away from being a part of our daily life activities due to insufficient control methods [5 and 6]. Since humanoid robots have usually high costs and the experiments are more laborious and dangerous than conventional robots, designing and validating advanced controllers and trajectories cannot be easily realized [7]. Dynamic simulators are very useful control tools in humanoid researches, since advanced control structures and trajectory patterns can be easily designed and validated [7 and 8]. However, designing a dynamic simulator for humanoid robots is quite challenging task due to highly nonlinear dynamic model, redundant mechanical structure, and lack of a fixed point against conventional robotic systems such as industrial robots [9].

The dynamic models of humanoid robots and environmental contact, such as sole and floor contact model, should be derived to design a dynamic simulator. Conventional dynamic model derivation methods have several disadvantages in the design of a humanoid robot simulator, e.g., the dynamic model suffers from discontinuity since the fixed point of the robot changes during locomotion and multiple, i.e., serial and parallel, kinematic solutions are used in single and double support phases, respectively [10 and 11]. Model simplifications, such as sub-dimensional dynamic models in frontal and sagittal planes, are generally used to analyze humanoid robots and design simple simulators; however, they cannot reflect the exact dynamic behavior and limits the performances of humanoid robots in implementations [12 and 13].

Many different robot simulators have been proposed due to the incontestable advantages, e.g., advanced control systems can be designed and validated in a reliable, safe and cost effective manner [7, 14 and 15]. However, dynamic simulators cannot exactly reflect the real world due to model simplifications, which is called as the reality gap in the literature [15 and 16]. Although comparison studies for dynamic simulators have been proposed, there is no a clear approach to compare efficiency of simulating humanoid robots [7 and 8]. The simulations can be significantly improved by considering the actual dynamics of humanoid robots, e.g., actuator dynamics, joint frictions and so on. However, none of the commercial software packages, such as Webot and Adams, can provide full control over all the features of interested [7, 8, and 17]. Therefore, designing a dynamic simulator can be very useful to reflect the exact dynamic behavior of humanoid robots and achieve high performance controllers [17].

ISSN: 2319-5967
ISO 9001:2008 Certified
International Journal of Engineering Science and Innovative Technology (IJESIT)
Volume 4, Issue 6, November 2015

In this paper, a new dynamic simulator is proposed for humanoid robots. A user can easily design advanced controllers thanks to its user friendly conventional control engineering-based schematic design. The proposed simulator can be modified by changing the design parameters, such as inertia of humanoid robot, and/or adding un-modeled dynamics, such as nonlinear friction and actuator dynamics, by users. Therefore, better dynamic models can be achieved to reflect the dynamic behavior of the actual robot and high performance advanced controllers can be designed for specific implementations. Without any approximation, the floating point base exact dynamic model of a humanoid robot is derived by using Newton-Euler algorithm and analytical derivation method so as to provide better insight into the dynamic behaviors of humanoid robots. Although only humanoid robots are considered in this manuscript, the proposal can be similarly applied to many different floating point base dynamic systems such as mobile and space robots. The model of environmental contact, specifically floor and sole contact model, is as important as the robot dynamics in the simulator design of a humanoid robot. A virtual spring-damper collision model is used to derive the dynamics of whole body contact model of a humanoid robot, since the contact forces can be uniquely obtained by using an impedance model which is very well-known by robotics researchers. A new dynamic simulator is designed by using the proposed dynamic models and MATLAB-Simulink. Animations are performed by using the Virtual Reality Toolbox (VRT) of MATLAB. Simulation results of whole body motion control of a humanoid robot are given to verify the proposal.

The rest of the paper is organized as follows. In section 2, the floating point base dynamic model of a humanoid robot is derived by using numerical and analytical methods. In section 3, contact forces of a humanoid robot are derived by using virtual spring-damper collision model. In section 4, new simulator is briefly introduced. In section 5, simulation results of whole body motion control of a humanoid robot are given. The paper ends with conclusion given in the last section.

II. DYNAMIC MODEL OF A HUMANOID ROBOT

In this section, the floating point base exact dynamic model of a humanoid robot is derived by using numerical and analytical methods.

Figure 1 shows a general structure for a humanoid robot which has four limbs connected to a free floating base link. The closed form dynamic model of a humanoid robot is derived as follows:

$$\begin{bmatrix} {}^{B}\mathbf{M}_{B} & {}^{B}\mathbf{M}_{L} \\ {}^{L}\mathbf{M}_{B} & {}^{L}\mathbf{M}_{L} \end{bmatrix} \underbrace{\begin{bmatrix} \ddot{\mathbf{x}}_{B} \\ \ddot{\mathbf{x}}_{L} \end{bmatrix}}_{\ddot{\mathbf{x}}} + \begin{bmatrix} \mathbf{c}_{B}(\mathbf{x},\dot{\mathbf{x}}) \\ \mathbf{c}_{L}(\mathbf{x},\dot{\mathbf{x}}) \end{bmatrix} + \begin{bmatrix} \mathbf{g}_{B}(\mathbf{x}) \\ \mathbf{g}_{L}(\mathbf{x}) \end{bmatrix} = \begin{bmatrix} \mathbf{0} \\ \boldsymbol{\tau}_{L} \end{bmatrix} + \mathbf{J}^{T}\mathbf{F}$$
$$\mathbf{J}_{m}\ddot{\mathbf{q}}_{m} = \boldsymbol{\tau}_{m} - \boldsymbol{\tau}_{frc} - \boldsymbol{\tau}_{m}^{dis} \tag{1}$$

where $\ddot{\mathbf{x}}_{B} = \begin{bmatrix} \dot{\mathbf{v}}^{T} & \dot{\mathbf{w}}^{T} \end{bmatrix}^{T}$ represents base-link accelerations in which $\dot{\mathbf{v}}$ and $\dot{\mathbf{w}}$ are linear and angular acceleration vectors, respectively; ${}^{B}\mathbf{M}_{B} = \begin{bmatrix} \mathbf{m}_{\dot{v}\dot{v}} & \mathbf{m}_{\dot{v}\dot{w}} \\ \mathbf{m}_{\dot{w}\dot{v}} & \mathbf{m}_{\dot{w}\dot{w}} \end{bmatrix}$ represents the inertia matrix of the base-link in which $\mathbf{m}_{\dot{v}\dot{v}}$, $\mathbf{m}_{\dot{w}\dot{w}}$ and $\mathbf{m}_{\dot{v}\dot{w}}$ are the inertia sub-matrices related to the linear and angular accelerations, respectively; $\ddot{\mathbf{x}}_{L}$ represents the accelerations of limbs' joints; ${}^{L}\mathbf{M}_{L} = \begin{bmatrix} \mathbf{m}_{11} & \cdots & \mathbf{m}_{1n} \\ \vdots & \cdots & \vdots \\ \mathbf{m}_{n1} & \cdots & \mathbf{m}_{nn} \end{bmatrix}$ represents the limbs' inertia matrix in which $\mathbf{m}_{ij}$ is the inertia sub-matrix related to the i^{th} and j^{th} limbs; ${}^{B}\mathbf{M}_{L} = {}^{L}\mathbf{M}_{B}{}^{T} = \begin{bmatrix} \mathbf{m}_{\dot{v}1} & \cdots & \mathbf{m}_{\dot{v}n} \\ \mathbf{m}_{\dot{w}2} & \cdots & \mathbf{m}_{\dot{w}n} \end{bmatrix}$ represents the non-diagonal inertia matrix in which $\mathbf{m}_{\dot{v}i}$ and $\mathbf{m}_{\dot{w}i}$ are the inertia sub-matrices related to the accelerations of the i^{th} limb and base-link linear and angular motions, respectively; $\mathbf{c}_{B}(\mathbf{x},\dot{\mathbf{x}})$ and $\mathbf{c}_{L}(\mathbf{x},\dot{\mathbf{x}})$ represent Coriolis and centrifugal force/torque vectors; $\mathbf{g}_{B}(\mathbf{x})$ and $\mathbf{g}_{L}(\mathbf{x})$ represent gravity force/torque vectors; $\boldsymbol{\tau}_{L}$ represents generalized torque vector of limbs' joints; $\mathbf{J}$ represents Jacobian matrix; $\mathbf{F}$ represents external forces and moments acting on the robot, such as the reaction force of floor; $\mathbf{J}_{m}$ represents diagonal inertia matrix of motors; $\ddot{\mathbf{q}}_{m}$ represents the vector of motor

ISSN: 2319-5967
ISO 9001:2008 Certified
International Journal of Engineering Science and Innovative Technology (IJESIT)
Volume 4, Issue 6, November 2015

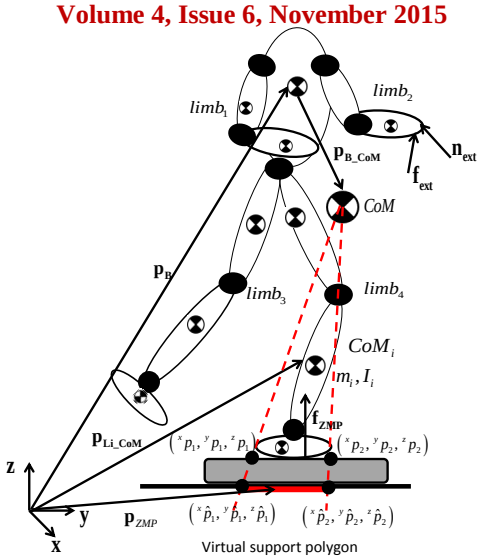

Fig.1: A general structure for a humanoid robot.

accelerations; and $\boldsymbol{\tau}_{\mathbf{m}}$, $\boldsymbol{\tau}_{\mathbf{frc}}$ and $\boldsymbol{\tau}_{\mathbf{m}}^{\mathbf{dis}}$ represent the vectors of motor, friction and external disturbance torques, respectively.

A. Numerical derivation method:

Since a humanoid robot has a highly redundant mechanical structure, derivation of Eq. (1) is not an easy task in general.
A numerical algorithm can be used to systematically derive the closed form dynamic model of a humanoid robot as follows:

Inertia Matrix:

1) Derivation of $\mathbf{m}_{\dot{\mathbf{v}}\dot{\mathbf{v}}}$, $\mathbf{m}_{\dot{\mathbf{w}}\dot{\mathbf{v}}}$ and $\mathbf{m}_{\dot{\mathbf{v}}i}$:

for j = 1 : 3

$$\dot{\mathbf{x}} = \mathbf{0}, \ddot{\mathbf{x}} = \mathbf{0}, \mathbf{g} = \mathbf{0}, \mathbf{F} = \mathbf{0} \quad (2)$$

$$\dot{\mathbf{v}}(j) = 1 \quad (3)$$

for i = 1 : n

$$\left[{}^{i}\mathbf{f}_{\mathbf{B}}, {}^{i}\mathbf{n}_{\mathbf{B}}, {}^{i}\boldsymbol{\tau}\right] = NE(i) \quad (4)$$

$$\mathbf{m}_{\dot{\mathbf{v}}i}{}^{T}(j) = {}^{i}\boldsymbol{\tau} \quad (5)$$

end

$$\hat{\mathbf{m}}_{\dot{\mathbf{v}}\dot{\mathbf{v}}}(j) = \sum_{i} {}^{i}\mathbf{f}_{\mathbf{B}}, \ \mathbf{m}_{\dot{\mathbf{w}}\dot{\mathbf{v}}}(j) = \sum_{i} {}^{i}\mathbf{n}_{\mathbf{B}} \quad (6)$$

$$\dot{\mathbf{x}} = \mathbf{0}, \ddot{\mathbf{x}} = \mathbf{0}, \mathbf{g} = \mathbf{0}, \mathbf{F} = \mathbf{0} \quad (7)$$

$$\dot{\mathbf{w}}(j) = 1 \quad (8)$$

for i = 1 : n

$$\left[{}^{i}\mathbf{f}_{\mathbf{B}}, {}^{i}\mathbf{n}_{\mathbf{B}}, {}^{i}\boldsymbol{\tau}\right] = NE(i) \quad (9)$$

$$\mathbf{m}_{\dot{\mathbf{w}}i}{}^{T}(j) = {}^{i}\boldsymbol{\tau} \quad (10)$$

end

$$\mathbf{m}_{\dot{\mathbf{v}}\dot{\mathbf{w}}}(j) = \sum_{i} {}^{i}\mathbf{f}_{\mathbf{B}}, \ \hat{\mathbf{m}}_{\dot{\mathbf{w}}\dot{\mathbf{w}}}(j) = \sum_{i} {}^{i}\mathbf{n}_{\mathbf{B}} \quad (11)$$

end

$$\mathbf{m}_{\dot{\mathbf{v}}\dot{\mathbf{v}}} = \hat{\mathbf{m}}_{\dot{\mathbf{v}}\dot{\mathbf{v}}} + m_B\mathbf{E}_3, \ \mathbf{m}_{\dot{\mathbf{w}}\dot{\mathbf{w}}} = \hat{\mathbf{m}}_{\dot{\mathbf{w}}\dot{\mathbf{w}}} + \mathbf{I}_{\mathbf{B}} \quad (12)$$

ISSN: 2319-5967
ISO 9001:2008 Certified
International Journal of Engineering Science and Innovative Technology (IJESIT)
Volume 4, Issue 6, November 2015

Where n represents the number of the limbs; $\mathbf{E}_3$ represents a 3x3 identity matrix; $\mathbf{I}_\mathbf{B}$ represents the inertia of the base-link; and $NE()$ represents the well-known Newton-Euler numerical algorithm that is widely used to derive the dynamic models of robots [18].

2) Derivation of $\mathbf{m}_{wi}$, $\mathbf{m}_{vi}$ and $\mathbf{m}_{ij}$:

for i = 1: n

$$\dot{\mathbf{x}} = \mathbf{0}, \ddot{\mathbf{x}} = \mathbf{0}, \mathbf{g} = \mathbf{0}, \mathbf{F} = \mathbf{0} \tag{13}$$

for j = 1 : i_k

$$\ddot{\mathbf{x}}_{\mathbf{limb}} = \mathbf{0} \tag{14}$$

$$^{\mathbf{i}}\ddot{\mathbf{x}}_{\mathbf{limb}}(j) = 1 \tag{15}$$

for k = 1 : n

$$\left[{}^k\mathbf{f}_\mathbf{B}, {}^k\mathbf{n}_\mathbf{B}, {}^k\boldsymbol{\tau}\right] = NE(k) \tag{16}$$

$$\mathbf{m}_{ki}(j) = {}^k\boldsymbol{\tau} \tag{17}$$

end

$$\mathbf{m}_{vi}(j) = \sum_k {}^k\mathbf{f}_\mathbf{B}, \ \mathbf{m}_{wi}(j) = \sum_k {}^k\mathbf{n}_\mathbf{B} \tag{18}$$

end

end

Where i_k represents the degrees-of-freedom in the i^{th} limb.

Hence, the inertia matrix is derived. The computational load can be decreased by using the symmetry property of the inertia matrix, i.e., $\mathbf{m}_{vw} = \mathbf{m}_{wv}^{\ T}$.

Coriolis and Centrifugal Vector:

$$\ddot{\mathbf{x}} = \mathbf{0}, \mathbf{g} = \mathbf{0}, \mathbf{F} = \mathbf{0} \tag{19}$$

for i = 1 : n

$$\left[{}^i\mathbf{f}_\mathbf{B}, {}^i\mathbf{n}_\mathbf{B}, {}^i\boldsymbol{\tau}\right] = NE(i) \tag{20}$$

end

$$\mathbf{c}_\mathbf{B}(\mathbf{x}, \dot{\mathbf{x}}) = \left[\sum_i {}^i\mathbf{f}_\mathbf{B}^{\ T}, \sum_i {}^i\mathbf{n}_\mathbf{B}^{\ T}\right]^T, \mathbf{c}_\mathbf{L}(\mathbf{x}, \dot{\mathbf{x}}) = \left[{}^1\boldsymbol{\tau}^T, \ \cdots, \ {}^n\boldsymbol{\tau}^T\right]^T \tag{21}$$

Gravity Vector:

Gravity vector is similarly derived by using Eq. (19-21) and

$$\dot{\mathbf{x}} = \mathbf{0}, \ddot{\mathbf{x}} = \mathbf{0}, \mathbf{g} = \begin{bmatrix} 0 & 0 & -9.8 \end{bmatrix}^T, \mathbf{F} = \mathbf{0} \tag{22}$$

Jacobian:

$$\dot{\mathbf{x}} = \mathbf{0}, \ddot{\mathbf{x}} = \mathbf{0}, \mathbf{g} = \mathbf{0} \tag{23}$$

for j = 1 : 6 x p

$$\mathbf{F} = \mathbf{0}, \ \mathbf{F}(j) = 1 \tag{24}$$

for i = 1 : n

$$\left[{}^i\mathbf{f}_\mathbf{B}, {}^i\mathbf{n}_\mathbf{B}, {}^i\boldsymbol{\tau}\right] = NE(i) \tag{25}$$

end

$$\mathbf{J}^T(j) = \left[\sum_i {}^i\mathbf{f}_\mathbf{B}^{\ T}, \sum_i {}^i\mathbf{n}_\mathbf{B}^{\ T}, {}^1\boldsymbol{\tau}^T \ \cdots \ {}^n\boldsymbol{\tau}^T\right]^T \tag{26}$$

end

where p represents the number of $\mathbf{F}$ acting on the robot.

ISSN: 2319-5967
ISO 9001:2008 Certified
International Journal of Engineering Science and Innovative Technology (IJESIT)
Volume 4, Issue 6, November 2015

B. Analytical derivation method:

In this sub-section, Eq. (1) is derived by proposing an analytical method. Although same result is obtained, the proposed analytical method provides better insight into the dynamic characteristics of humanoid robots.

Diagonal Terms of Inertia Matrix:

If it is assumed that $\dot{\mathbf{x}} = \mathbf{0}, \ddot{\mathbf{x}} = \mathbf{0}$ and $\mathbf{g} = \mathbf{0}$ except $\dot{\mathbf{v}}$, then the total inertial force acting on the robot is derived as follows:

$$\mathbf{F}_{\text{total}} = \mathbf{m}_{\dot{\mathbf{v}}\dot{\mathbf{v}}} \dot{\mathbf{v}} \tag{27}$$

where $\mathbf{m}_{\dot{\mathbf{v}}\dot{\mathbf{v}}} = \left(m_B + \sum_i m_i \right) \mathbf{E}_3$. (28)

Let us consider $\dot{\mathbf{x}} = \mathbf{0}, \ddot{\mathbf{x}} = \mathbf{0}$ and $\mathbf{g} = \mathbf{0}$ except $\dot{\mathbf{w}}$ instead of $\dot{\mathbf{v}}$. Total inertial moment acting on the robot due to angular acceleration is derived as follows:

$$\boldsymbol{\tau}_{\text{total}} = \mathbf{m}_{\dot{\mathbf{w}}\dot{\mathbf{w}}} \dot{\mathbf{w}} \tag{29}$$

The sub-inertia matrix $\mathbf{m}_{\dot{\mathbf{w}}\dot{\mathbf{w}}}$ is the total inertia of the robot and is derived by using the parallel axis theorem as follows:

$$\mathbf{m}_{\dot{\mathbf{w}}\dot{\mathbf{w}}} = \mathbf{I}_B + \sum_i \left({}_i\mathbf{R}\, {}^i\mathbf{I}_{c_i}\, {}_i\mathbf{R}^T + \left(\mathbf{p}_{B\_CoM_i}{}^T \mathbf{p}_{B\_CoM_i} \right) \mathbf{E}_3 - \mathbf{p}_{B\_CoM_i}\, \mathbf{p}_{B\_CoM_i}{}^T \right) \tag{30}$$

where $\mathbf{p}_{B\_CoM_i}$ represents a vector from base-link to the CoM of the i^{th} link.

Finally, if it is assumed that $\dot{\mathbf{x}} = \mathbf{0}, \ddot{\mathbf{x}} = \mathbf{0}$ and $\mathbf{g} = \mathbf{0}$ except $\ddot{\mathbf{x}}_{\mathbf{L}}$, then the inertia matrices of limbs are derived by using Lagrangian as follows:

$$\mathbf{m}_{ii} = \sum_i \left(m_i \mathbf{J}_{V_{CoMi}}{}^T \mathbf{J}_{V_{CoMi}} + \mathbf{J}_{W_{CoMi}}{}^T\, {}_i\mathbf{R}\, {}^i\mathbf{I}_i\, {}_i\mathbf{R}^T \mathbf{J}_{W_{CoMi}} \right) \tag{31}$$

where $\mathbf{J}_{V_{CoMi}}$ and $\mathbf{J}_{W_{CoMi}}$ represent linear and angular Jacobian matrices of the i^{th} link's CoM, respectively.

Non-Diagonal Terms of Inertia Matrix:

Let us again consider $\dot{\mathbf{x}} = \mathbf{0}, \ddot{\mathbf{x}} = \mathbf{0}$ and $\mathbf{g} = \mathbf{0}$ except $\dot{\mathbf{w}}$. The total force acting on the robot due to angular acceleration is derived as follows:

$$\mathbf{F}_{\text{total}} = \mathbf{m}_{\dot{\mathbf{v}}\dot{\mathbf{w}}} \dot{\mathbf{w}} \tag{32}$$

$$\mathbf{F}_{\text{total}} = \left(m_B + \sum_i m_i \right) \dot{\mathbf{v}}_{\text{CoM}} = \left(m_{body} + \sum_i m_i \right) \left(\mathbf{p}_{B\_CoM} \right)_\times \dot{\mathbf{w}} \tag{33}$$

where $\mathbf{p}_{B\_CoM}$ represents a vector from base-link to the robot's CoM; and $(\bullet)_\times$ represents skew-symmetric matrix.

Finally, if it is again assumed that $\dot{\mathbf{x}} = \mathbf{0}, \ddot{\mathbf{x}} = \mathbf{0}$ and $\mathbf{g} = \mathbf{0}$ except $\ddot{\mathbf{x}}_{\mathbf{L}}$, then total inertial force and moment acting on the base-link are derived as follows:

$$\mathbf{F}_{\text{total}} = \sum_j \mathbf{m}_{\dot{\mathbf{v}}j}\, {}^j\ddot{\mathbf{x}}_{\mathbf{L}} \tag{34}$$

$$\boldsymbol{\tau}_{\text{total}} = \sum_j \mathbf{m}_{\dot{\mathbf{w}}j}\, {}^j\ddot{\mathbf{x}}_{\mathbf{L}} \tag{35}$$

Consequently, the inertial sub-matrices $\mathbf{m}_{\dot{\mathbf{v}}j}$ and $\mathbf{m}_{\dot{\mathbf{w}}j}$ are derived as follows:

$$\mathbf{m}_{\dot{\mathbf{v}}j} = \sum_j m_j \mathbf{J}_{V_{CoMj}} \tag{36}$$

$$\mathbf{m}_{\dot{\mathbf{w}}j} = \sum_j \left({}^0_j\mathbf{R}\, {}^i\mathbf{I}_i\, {}^0_j\mathbf{R}^T \mathbf{J}_{W_{CoMi}} + m_j \left(\mathbf{p}_{B\_CoM_j} \right)_\times \mathbf{J}_{V_{CoMj}} \right) \tag{37}$$

Since the accelerations of a limb do not directly influence the other limbs' motions, $\mathbf{m}_{ij} = \mathbf{0}$ when $i \neq j$.

ISSN: 2319-5967
ISO 9001:2008 Certified
International Journal of Engineering Science and Innovative Technology (IJESIT)
Volume 4, Issue 6, November 2015

Gravity

$$\mathbf{g}_B = 9.8\left[\left(m_B + \sum_i m_i\right)\mathbf{v}_g{}^T, \sum_i m_i\left(\left(\mathbf{p}_{Li\_CoM} - \mathbf{p}_B\right)\times\mathbf{v}_g\right)^T\right]^T \tag{38}$$

$$\mathbf{g}_{L_j} = 9.8\sum_i {}^j m_i\ {}^j\mathbf{J}_{VCoM_i}{}^T\mathbf{v}_g \tag{39}$$

$$\mathbf{g} = [\mathbf{g}_B{}^T,\ \mathbf{g}_{L_1}{}^T,\ \cdots,\ \mathbf{g}_{L_n}{}^T]^T \tag{40}$$

Jacobian

Jacobian is derived for the tip point of the r[th] limb as follows:

$${}^r\mathbf{J}_{V_1} = \mathbf{E}_3,\ {}^r\mathbf{J}_{V_2} = \left[[1,0,0]^T\times\mathbf{p}_{B\_{}^rL_{tip}}, [0,1,0]^T\times\mathbf{p}_{B\_{}^rL_{tip}}, [0,0,1]^T\times\mathbf{p}_{B\_{}^rL_{tip}}\right] \tag{41}$$

$${}^r\mathbf{J}_{V_k} = \begin{cases}\left[\mathbf{w}_1\times\mathbf{p}_{j1\_{}^rL_{tip}}, \mathbf{w}_2\times\mathbf{p}_{j2\_{}^rL_{tip}}, \cdots, \mathbf{w}_{r_k}\times\mathbf{p}_{jr_k\_{}^rL_{tip}}\right] & if\ r = k\\ \mathbf{0} & otherwise\end{cases} \tag{42}$$

$${}^r\mathbf{J}_{W_1} = \mathbf{0}_3,\ {}^r\mathbf{J}_{W_2} = \mathbf{E}_3 \tag{43}$$

$${}^r\mathbf{J}_{W_k} = \begin{cases}\left[\mathbf{w}_1, \mathbf{w}_2, \cdots \mathbf{w}_{r_k}\right] & if\ r = k\\ \mathbf{0} & otherwise\end{cases} \tag{44}$$

$${}^r\mathbf{J} = \begin{bmatrix}{}^r\mathbf{J}_{V_1} & \cdots & {}^r\mathbf{J}_{V_{r_k}}\\ {}^r\mathbf{J}_{W_1} & \cdots & {}^r\mathbf{J}_{W_{r_k}}\end{bmatrix} \tag{45}$$

where $\mathbf{p}_{B\_{}^rL_{tip}}$ represents the distance between tip point of the r[th] limb and body; ${}^r\mathbf{p}_{ji\_{}^rL_{tip}}$ represents the distance between tip point of the r[th] limb and joint i; and r_k represents the degrees-of-freedom of the r[th] limb. Equations (27-45) show that Eq. (1) can be analytically derived except Coriolis and centrifugal force/torque vector without any approximation.

III. CONTACT MODEL OF A HUMANOID ROBOT AND ENVIRONMENT

In the dynamic simulation of a humanoid robot, the model of environmental contact is as important as the dynamic model of the robot. In this section, the contact between floor and sole is modeled by using virtual spring-damper collision model. Although only floor and sole contact is considered in this section, the proposed model can be similarly used for the whole body contact motion.

The reaction horizontal and vertical forces, which include impact forces that occur when contact starts, are the main external forces that are applied on a humanoid robot during bipedal locomotion. Since virtual spring-damper collision model has several advantages, e.g., friction and impact forces can be obtained by using a unique model and contact can be intuitively described by using the impedance of environment, it is used in the design of dynamic simulator [19].

The contact model of a humanoid robot's sole and floor is illustrated in Fig. 2. For the sake of simplicity, only four contact points at the corners of the sole are considered as shown in Fig. 2a. In practice, many humanoid robots use force sensors at the corner of the soles to estimate reaction floor forces or zero moment points [20 and 21]. It is assumed that each corner of the sole has three virtual spring-damper models in the perpendicular x, y and z coordinate directions. They are formulized as follows:

$$\mathbf{F}_{x_i} = -D_{floor}\Delta\dot{\mathbf{x}}_i - K_{floor}\Delta\mathbf{x}_i \tag{46}$$

$$\mathbf{F}_{y_i} = -D_{floor}\Delta\dot{\mathbf{y}}_i - K_{floor}\Delta\mathbf{y}_i \tag{47}$$

$$\mathbf{F}_{z_i} = -D_{floor}\Delta\dot{\mathbf{z}}_i - K_{floor}\Delta\mathbf{z}_i \tag{48}$$

ISSN: 2319-5967
ISO 9001:2008 Certified
International Journal of Engineering Science and Innovative Technology (IJESIT)
Volume 4, Issue 6, November 2015

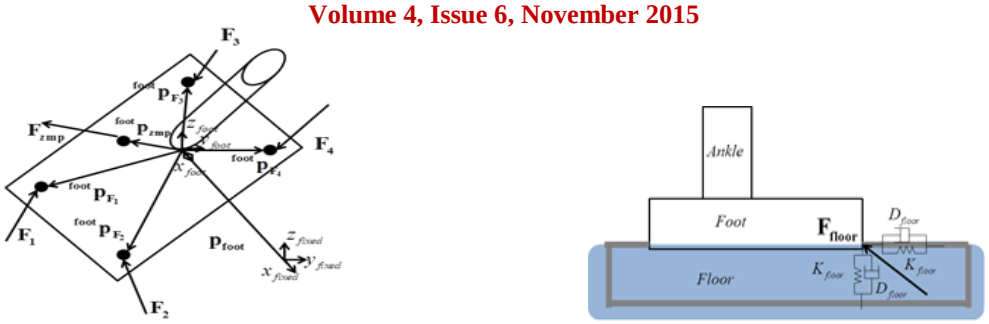

a) Applied forces at sole **b) Contact model**

Fig. 2: Sole-floor contact model and applied forces at sole

Where D_{floor} and K_{floor} represent the floor's damping and stiffness coefficients, respectively; and $\Delta\mathbf{x}_i, \Delta\mathbf{y}_i, \Delta\mathbf{z}_i$ and $\Delta\dot{\mathbf{x}}_i, \Delta\dot{\mathbf{y}}_i, \Delta\dot{\mathbf{z}}_i$ represent the relative positions and velocities in the x, y and z coordinate directions at point i, respectively.

If there is slipping, in which horizontal forces are larger than the maximum static frictional force that is $\mu_s \mathbf{F}_{z_i}$, then Eq. (46) and Eq. (47) are re-written as follows:

$$\mathbf{F}_{x_i} = \mu_d \left|\mathbf{F}_{z_i}\right| \frac{\Delta\mathbf{x}_i}{\left|\Delta\mathbf{x}_i\right|} \tag{49}$$

$$\mathbf{F}_{y_i} = \mu_d \left|\mathbf{F}_{z_i}\right| \frac{\Delta\mathbf{y}_i}{\left|\Delta\mathbf{y}_i\right|} \tag{50}$$

Where μ_s and μ_d represent static and dynamic friction coefficients, respectively. The zero moment point (ZMP), which is a widely used stability/equilibrium criterion in dynamic walking, of the humanoid robot can be easily derived as follows:

$$\mathbf{p}_{ZMP} = \frac{\sum_{i=1}^{4} \mathbf{p}_{f_i} \left|\mathbf{F}_{z_i}\right|}{\sum_{i=1}^{4} \left|\mathbf{F}_{z_i}\right|} = \sum_{i=1}^{4} \mathbf{p}_{f_i} \frac{\left|\mathbf{F}_{z_i}\right|}{\left|\mathbf{F}_{z}\right|} \tag{51}$$

The external force and moment acting on the foot are derived as follows:

$$\mathbf{F}_{foot} = \mathbf{F}_{ZMP} = \sum_{i=1}^{4} \mathbf{F}_i, \quad \boldsymbol{\tau}_{foot} = \left(\mathbf{p}_{ZMP} - \mathbf{p}_{foot}\right) \times \mathbf{F}_{ZMP} \tag{52}$$

IV. NEW DYNAMIC SIMULATOR DESIGN

In this section, a new dynamic simulator for humanoid robots is presented. MATLAB-Simulink, which is one of the most widely, used development environments for numerical computing in the robotics community and the proposed dynamic model are used in the design of the simulator [22].

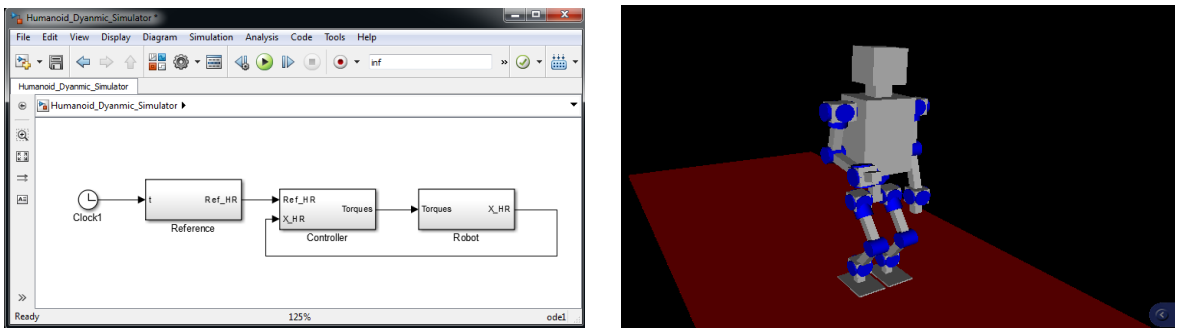

a) Control block diagram in Simulink **b) Humanoid robot animation in Virtual Reality Toolbox**

Fig. 3: Proposed dynamic simulator.

ISSN: 2319-5967
ISO 9001:2008 Certified
International Journal of Engineering Science and Innovative Technology (IJESIT)
Volume 4, Issue 6, November 2015

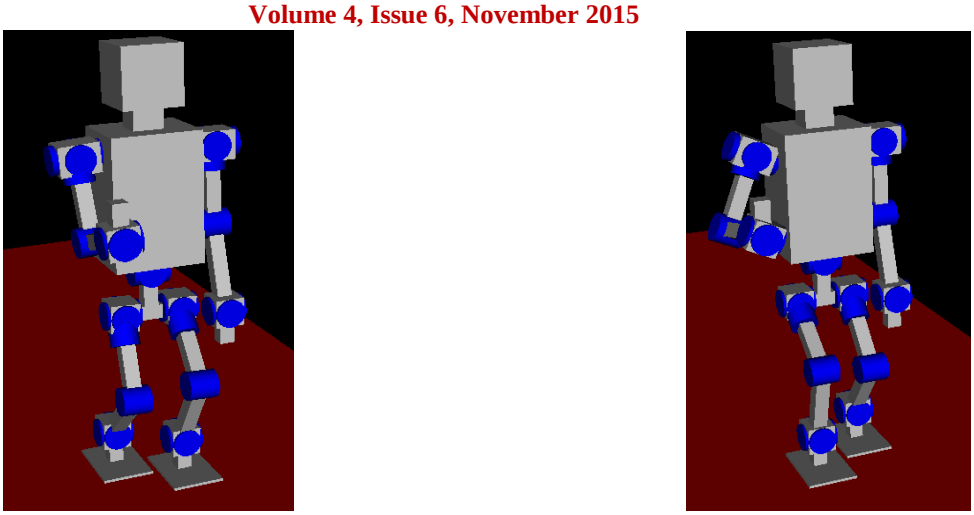

(a) t = 1.53 s. **(b) t = 4.35 s.**

Fig. 4: Dynamic walking on an even terrain.

The block diagram of the proposed dynamic simulator is shown in Fig. 3a. In this figure, the block of "Robot" represents the dynamic models given in sections II and III, the block of "Controller" represents any motion controller that is designed by users, e.g., a ZMP controller, the block of "Reference" represents any reference input that is generated by considering the control goals, e.g., ZMP trajectory generation, and "X_HR" represents the states of the Humanoid Robot, e.g., the joint angles and velocities of the robot. The dynamic simulator is designed by using the conventional control engineering schematic diagram so as to provide a user friendly interface. A researcher who has basic control knowledge can easily adapt and use the proposed dynamic simulator. Moreover, it can be easily improved by using many different tools of MATLAB-Simulink, e.g., the singularity of the robot can be easily analyzed by using MATLAB's eigenvalue function. Against the commercial dynamic simulator software packages, not only the design parameters but also the un-modeled dynamics, such as nonlinear friction disturbances at joints and actuator dynamics, can be directly modified by users. Therefore, better simulation results can be achieved and high performance controllers can be designed for specific applications as suggested in [17]. Fig. 3b shows the humanoid robot that is designed by using the Virtual Reality Toolbox (VRT) of MATLAB-Simulink. It should be noted here that advanced CAD models can be similarly used to animate robots in VRT [23].

V. SIMULATION RESULTS

In this section, whole body motion controllers are designed for a humanoid robot so as to show the efficiency of the simulator and validate the proposal.

Let us start by considering the dynamic walking problem of the humanoid robot. ZMP is one of the most widely used dynamic walking stability/equilibrium criterion in bipedal locomotion [24]. The CoM trajectories of the humanoid robot, which satisfy stable dynamic walking, are derived by using ZMP as follows:

$$
\begin{aligned}
{}^{x}p_{CoM}(t) &= \left({}^{x}p_{CoM}(t_0) - {}^{x}p_{ZMP}\right)\cosh\left(\omega(t-t_0)\right) + \frac{{}^{x}\dot{p}_{CoM}(t_0)}{\omega}\sinh\left(\omega(t-t_0)\right) + {}^{x}p_{ZMP} \\
{}^{x}\dot{p}_{CoM}(t) &= \omega\left({}^{x}p_{CoM}(t_0) - {}^{x}p_{ZMP}\right)\sinh\left(\omega(t-t_0)\right) + {}^{x}\dot{p}_{CoM}(t_0)\cosh\left(\omega(t-t_0)\right) \\
{}^{x}\ddot{p}_{CoM}(t) &= \omega^2\left({}^{x}p_{CoM}(t_0) - {}^{x}p_{ZMP}\right)\cosh\left(\omega(t-t_0)\right) + \omega\,{}^{x}\dot{p}_{CoM}(t_0)\sinh\left(\omega(t-t_0)\right)
\end{aligned}
\tag{53}
$$

where ${}^{x}p_{CoM}(t)$ and ${}^{x}p_{ZMP}$ represent the positions of CoM and ZMP in x direction, respectively; and $\omega = \sqrt{g/{}^{z}p_{CoM}}$ in which g represents gravitational acceleration.

An acceleration-based position controller is designed for the CoM of the humanoid robot as follows:

$$
{}^{x}\ddot{p}^{des}_{CoM}(t) = {}^{x}\ddot{p}^{ref}_{CoM}(t) + K_D\left({}^{x}\dot{p}^{ref}_{CoM}(t) - {}^{x}\dot{p}_{CoM}(t)\right) + K_P\left({}^{x}p^{ref}_{CoM}(t) - {}^{x}p_{CoM}(t)\right) \tag{54}
$$

ISSN: 2319-5967
ISO 9001:2008 Certified
International Journal of Engineering Science and Innovative Technology (IJESIT)
Volume 4, Issue 6, November 2015

where ${}^{x}\ddot{p}_{CoM}^{ref}(t)$ and ${}^{x}\ddot{p}_{CoM}^{des}(t)$ represent reference and desired CoM trajectories, respectively.

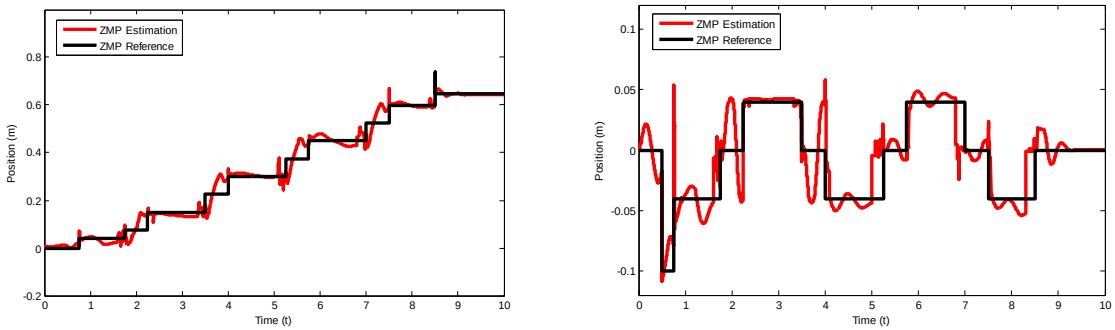

(a) ZMP in x direction. **(b) ZMP in y direction.**

Fig. 5: ZMP in horizontal plane when robot walks on the even terrain.

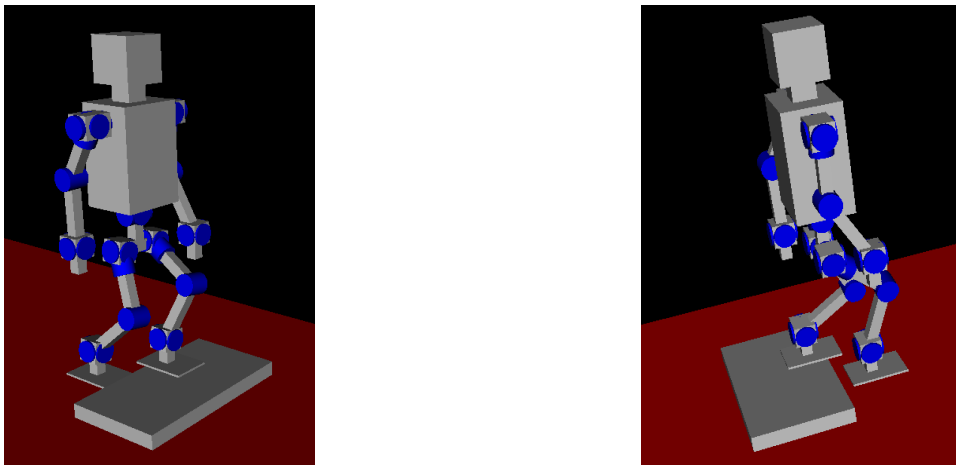

(a) t = 2.5 s. **(b) t = 6.5 s.**

Fig. 6: Dynamic walking on an uneven terrain.

The torques of the robot joints are obtained, i.e., the motion controller is designed, by using the desired CoM trajectories and the proposed dynamic model. Figure 4 shows the whole body motion control simulation results when the humanoid robot walks on an even terrain and waves its right hand. The ZMP reference trajectories and measurements are shown in Fig. 5. Figure 4 and Fig. 5 directly show that the ZMP of the humanoid robot can follow the reference trajectories and stable dynamic walking is achieved by using the proposed controller.

Let us again consider the dynamic walking problem when the humanoid robot walks on an un-even terrain. ZMP equations can be similarly used for an un-even terrain; however, the support polygon should be modified as shown in [20]. To achieve stable dynamic walking, ZMP should be kept in the virtual support polygon that is shown in Fig. 1.

Figure 6 shows the whole body motion control simulation results when the humanoid robot walks on an un-even terrain and robot arms move to suppress yaw moment and improve the stability [25]. The CoM reference trajectories and measurements are shown in Fig. 7. Figure 6 and Fig. 7 directly show that the CoM of the humanoid robot can follow the reference trajectories and stable dynamic walking is achieved by using the proposed controller.

ISSN: 2319-5967
ISO 9001:2008 Certified
International Journal of Engineering Science and Innovative Technology (IJESIT)
Volume 4, Issue 6, November 2015

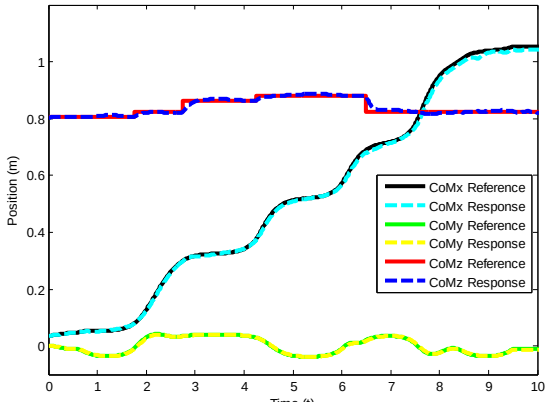

Fig.7: CoM of the humanoid robot when it walks on the uneven terrain.

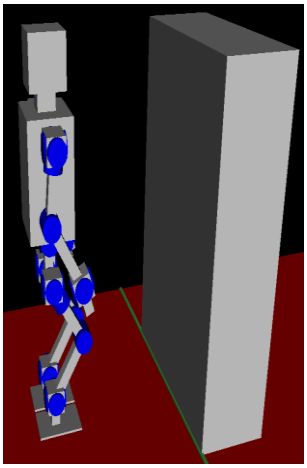

(a) t = 0 s.

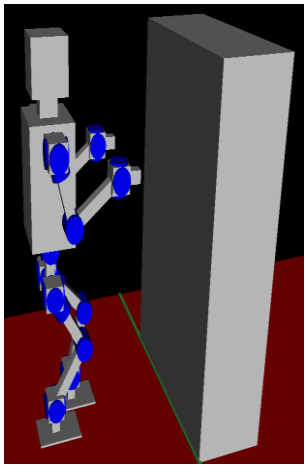

(b) t = 2.05 s.

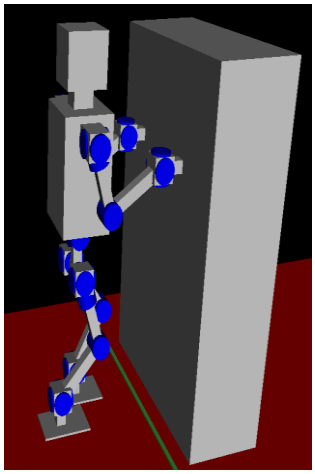

(c) t = 4.25 s.

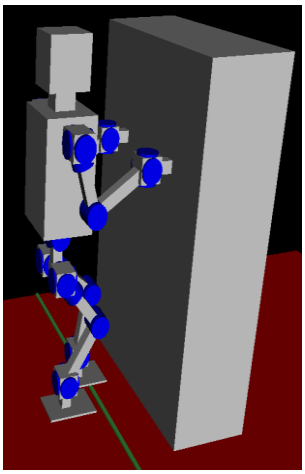

(d) t = 6 s.

Fig.8: Contact with environment.

So far, only the lower body contact motion, i.e., bipedal locomotion has been considered. However, upper body contact motion is as important as the lower body motion to perform dexterous and versatile tasks. Contact motion

ISSN: 2319-5967
ISO 9001:2008 Certified
International Journal of Engineering Science and Innovative Technology (IJESIT)
Volume 4, Issue 6, November 2015

control is a quite challenging issue due to the safety and performance limitation problems in force control [26 and 27].

Fig. 8 shows simulation results for the upper body contact motion control of the humanoid robot. In this simulation, the humanoid robot walks towards an obstacle and safely contacts and pushes it. Environmental contact forces are similarly obtained by using the virtual spring-damper collision model that is proposed in section III. Simulation results show that the proposed simulator can be used to design different high performance motion control systems and perform many different complicated tasks. Since not only the controller and reference trajectory but also the dynamic model of the robot and environment can be adjusted by users, better dynamic model approximation of the actual system can be obtained for the specific applications of humanoid robots. Therefore, more reliable high performance motion controllers can be designed by using the proposed simulator.

VI. CONCLUSION

In this paper, a new dynamic simulator is proposed for humanoid robots. Although only humanoid robots are considered, the proposal can be directly applied to many different floating point base dynamic systems, such as mobile robots. Conventional dynamic model derivation methods suffer from discontinuity problem when they are applied to such systems. An exact dynamic model of a humanoid robot is derived by proposing numerical and analytical methods. The proposal provides a unique model and better insight into the dynamic behavior of humanoid robots. A new dynamic simulator is designed by using the proposed dynamic model and MATLAB-Simulink. A user can easily adapt and use the proposed dynamic simulator thanks to its user friendly conventional control engineering-based schematic design. Moreover, the dynamic model can be modified by users so more reliable high performance motion controllers can be designed for the specific applications of humanoid robots. Animations are performed by using the Virtual Reality Toolbox of MATLAB. Whole body motion control simulation results of a humanoid robot are given to validate the proposal.

REFERENCES

[1] Sakagami, Y.; Watanabe, R.; Aoyama, C.; Matsunaga, S.; Higaki, N.; Fujimura, K., "The intelligent ASIMO: system overview and integration," IEEE/RSJ Int. Conf. on Intelligent Robots and Systems, pp. 2478-2483, 2002.

[2] Stiefelhagen, R.; Ekenel, H.K.; Fugen, C.; Gieselmann, P.; Holzapfel, H.; Kraft, F.; Nickel, K.; Voit, M.; Waibel, Alex, "Enabling Multimodal Human–Robot Interaction for the Karlsruhe Humanoid Robot," Robotics, IEEE Transactions on, vol.23, no.5, pp.840-851, Oct. 2007.

[3] Yongwook C.; Jaeseung J.; Sungho J., "Toward Brain-Actuated Humanoid Robots: Asynchronous Direct Control Using an EEG-Based BCI," Robotics, IEEE Transactions on, vol.28, no.5, pp.1131-1144, Oct. 2012.

[4] KangGeon K.; Young-Su C.; Jung-Min P.; Ji-Yong L.; Bum-Jae Y., "Providing services using network-based humanoids in a home environment," Consumer Electronics, IEEE Transactions on, vol.57, no.4, pp.1628-1636, Nov. 2011.

[5] Durán B.; Thill S., "Rob's Robot: Current and Future Challenges for Humanoid Robots," The Future of Humanoid Robots - Research and Applications, Dr. Riadh Zaier (Ed.), ISBN: 978-953-307-951-6, InTech, DOI: 10.5772/27197.

[6] Ohashi, E.; Aiko, T.; Tsuji, T.; Nishi, H.; Ohnishi, K., "Collision Avoidance Method of Humanoid Robot With Arm Force," Industrial Electronics, IEEE Transactions on, vol.54, no.3, pp.1632-1641, June 2007.

[7] T. Laue, M. Hebbel, "Automatic Parameter Optimization for a Dynamic Robot Simulation," L Iocchi et aL (Eds.), RoboCup 2008, LNAI 5399, pp. 121-132, 2009.

[8] Shafii, N.; Reis, L.P.; Rossetti, R.J.F., "Two humanoid simulators: Comparison and synthesis," Information Systems and Technologies (CISTI), 2011 6th Iberian Conference on , vol., no., pp.1,6, 15-18 June 2011.

[9]. E. Sariyildiz, H. Temeltas, "An Exact Dynamic Model for the Thomas-K Biped Robot: New Simulator Design", IEEE International Conference on Mechatronics and Automation (ICMA), Tianjin, China, 3-6 August 2014.

[10] Khosravi, B.; Yurkovich, S.; Hemami, H., "Control of a Four-Link Biped in a Back Somersault Maneuver," Systems, Man and Cybernetics, IEEE Transactions on, vol.17, no.2, pp.303-311, Mar. 1987.

[11] Hernández-Santos C; Rodriguez-Leal E.; Soto R.; Gordillo J.L., "Kinematics and Dynamics of a New 16 DOF Humanoid Biped Robot with Active Toe Joint". Int J Adv Robot Syst, vol. 9, 190:2012, Nov. 2012.

[12] S. Lee, C. Cho, M. T. C, M. Kim, J. Kim, "A Dynamic Model of Humanoid Robots using the Analytical Method", International Journal of Precision Engineering and Manufacturing, vol. 11, No. 1, pp. 67-75, Feb. 2010.

ISSN: 2319-5967
ISO 9001:2008 Certified
International Journal of Engineering Science and Innovative Technology (IJESIT)
Volume 4, Issue 6, November 2015

[13] Y. Hurmuzlu, F.Genot, B Brogliato, "Modeling, stability and control of biped robots—a general framework", Automatic 40 (2004) 1647 – 1664.

[14] S. Kucuk, "Simulation and design tool for performance analysis of planar parallel manipulators", Simulation: Transactions of the Society for Modeling and Simulation International, 88(5), 542–556, 2012.

[15] C. Zagal, 1. Ruiz, "Combining Simulation and Reality in Evolutionary Robotics," Journal of Intelligent and Robotic Systems, VoL50 (1), pp. 19-39, 2007.

[16] S. Koos, 1.-8. Mouret, "Crossing the reality gap in evolutionary robotics by promoting transferable controllers," Proc. 12th annual conference on Genetic and evolutionary computation, pp. 119-126, 2010.

[17] Medrano-Cerda, G.A.; Dallali, H.; Brown, M.; Tsagarakis, N.G.; Caldwell, D.G., "Modelling and simulation of the locomotion of humanoid robots," Control 2010, UKACC International Conference on, 7-10 Sept. 2010.

[18] J. Craig, "Introduction to robotics: Mechanics and Control", Prentice Hall, 3rd edt. 2004.

[19] Fujimoto Y.; Kawamura A, "Simulation of an Autonomous Biped Walking Robot Including Environmental Force Interaction", IEEE Robotics and Automation Magazine, vol. 5, no. 2, pp. 33-42, 1998.

[20] Sato, T.; Sakaino, S.; Ohashi, E.; Ohnishi, K., "Walking Trajectory Planning on Stairs Using Virtual Slope for Biped Robots," Industrial Electronics, IEEE Transactions on, vol.58, no.4, pp.1385-1396, April 2011.

[21] Barkan Ugurlu, and Atsuo Kawamura, "Bipedal Trajectory Generation based on Combining Inertial Forces and Intrinsic Angular Momentum Rate Changes: Eulerian ZMP Resolution", IEEE Transactions on Robotics, vol. 28, no. 6, December 2012, pp. 1406-1415.

[22] B. Inner and S. Kucuk, "A novel kinematic design, analysis and simulation tool for general Stewart platforms", Simulation: Transactions of the Society for Modeling and Simulation International, 89(7) 876–897.

[23] E. Sariyildiz, H. Temeltas, "A New Formulation Method for Solving Kinematic Problems of Multi-Arm Robot Systems Using Quaternion Algebra in the Screw Theory Framework" , Tr. J. Elec. Eng. & Comp. Sci., 2012, vol. 20, no.4, 607-628.

[24] Kajita S.; Tani K., "Study of dynamic biped locomotion on rugged terrain-derivation and application of the linear inverted pendulum mode," IEEE Internat.Conf. on Robotics & Automation, pp.1405-1411, 1991.

[25] Zhang S.; Huang Q.; Wang H.,; Xu W.; Ma G.; Liu Y.; Yu Z., "The Mechanism of Yaw Torque Compensation in the Human and Motion Design for Humanoid Robots". Int J Adv Robot Syst, vol. 10, 57:2013, Jan. 2013.

[26] Sariyildiz E.; Ohnishi K., "On the Explicit Robust Force Control via Disturbance Observer", Industrial Electronics, IEEE Transactions on, Mar. 2015, vol. 62, no. 3, pp. 1581-1589.

[27] Sariyildiz E.; Ohnishi, K., "An Adaptive Reaction Force Observer Design", Mechatronics IEEE/ASME Transaction on, vol. 20, no. 2, pp. 750-760, Apr. 2015.